Weather Radar Network Benefit Model for Nontornadic Thunderstorm Wind Casualty Cost Reduction

JOHN Y. N. CHO[a] AND JAMES M. KURDZO

Lincoln Laboratory, Massachusetts Institute of Technology, Lexington, Massachusetts

(Manuscript received 22 May 2020, in final form 27 August 2020)

ABSTRACT: An econometric geospatial benefit model for nontornadic thunderstorm wind casualty reduction is developed for meteorological radar network planning. Regression analyses on 22 years (1998–2019) of storm event and warning data show, likely for the first time, a clear dependence of nontornadic severe thunderstorm warning performance on radar coverage. Furthermore, nontornadic thunderstorm wind casualty rates are observed to be negatively correlated with better warning performance. In combination, these statistical relationships form the basis of a cost model that can be differenced between radar network configurations to generate geospatial benefit density maps. This model, applied to the current contiguous U.S. weather radar network, yields a benefit estimate of \$207 million (M) yr^{-1} relative to no radar coverage at all. The remaining benefit pool with respect to enhanced radar coverage and scan update rate is about \$36M yr^{-1}. Aggregating these nontornadic thunderstorm wind results with estimates from earlier tornado and flash flood cost reduction models yields a total benefit of \$1.12 billion yr^{-1} for the present-day radars and a remaining radar-based benefit pool of \$778M yr^{-1}.

KEYWORDS: North America; Severe storms; Radars/Radar observations; Regression analysis; Economic value; Geographic information systems (GIS)

1. Introduction

How much are meteorological radars worth to society? Data from weather radars have become a commonplace feature in everyday life (e.g., Saunders et al. 2018). Broadcast meteorologists use ''Doppler radar'' video loops for illustration, and people consult the latest weather radar images on their smart phones while contemplating the timing of their outdoor activities. Behind the scenes, these radars generate crucial information that leads to better numerical weather predictions and help meteorologists make severe weather warning decisions (e.g., Stensrud et al. 2009). Meteorological radars, however, are costly to acquire, operate, and maintain. As we make plans for future sensor networks, including replacement of the current weather radars, benefit monetization is needed to evaluate the trade-off between performance and cost (Hondl and Weber 2019).

The chains of causality that link weather radars to societal benefits are vast and complex. We began our investigation by focusing on a literally existential outcome—human casualties. Past studies have shown that timely National Weather Service (NWS) warnings can reduce casualties in the cases of tornadoes (Simmons and Sutter 2008) and flash floods (e.g., DeKay and McClelland 1993). Confirming and precisely quantifying these associations, and firmly establishing statistical relationships between radar coverage and warning performance, we were able to develop econometric geospatial weather radar benefit models for tornado (Cho and Kurdzo 2019a,b, hereinafter CK19a,b) and flash flood (Cho and Kurdzo 2020, hereinafter CK20) casualty reduction.

In this paper we extend our benefit model to nontornadic severe thunderstorm (SVR) wind casualties. While fatalities due to nontornadic thunderstorm wind events are fewer than those caused by tornadoes or flash floods, the total casualty count (including injuries) is greater than for flash floods (but lower than for tornadoes; Fig. 1). Hail events were also considered for inclusion in the model; however, as noted in section 2d, a lack of negative correlation between SVR warning performance and casualty rate for those events precluded their incorporation into the model. (Although non–flash floods are another significant source of casualties, they were examined and disregarded by CK20, since a statistical linkage could not be established between radar coverage and non-flash-flood-warning performance.)

Severe thunderstorms, as defined by the NWS, must meet one or more of three thresholds: production of a tornado, winds of at least 50 kt (25.8 m s^{-1}), and/or hail of at least 1 in. (=2.54 cm) in diameter (note that the hail threshold was increased from 0.75 to 1 in. in 2010 because of public-perceived overwarning for hail). Nontornadic severe thunderstorms are any severe thunderstorm that produces one or both of the wind and hail threshold exceedances for a severe thunderstorm, but not a tornado (Kelly et al. 1985). In general, the NWS issues SVR warnings for storms that appear likely to produce high winds and/or large hail but do not appear to be potentially tornadic. For wind events specifically, NWS forecasters generally use radar data and/or spotter reports of measured/estimated wind speed or damage (Lemon et al. 1977; Polger et al. 1994). Since the warnings are for the public at ground level, better radar observations at lower levels will generally yield more accurate estimates for warning issuance. In addition to near-ground-level wind observations, forecasters also utilize volumetric radar data to identify descending reflectivity cores in order to predict/warn for microburst winds (Roberts and Wilson 1989).

[a] ORCID: 0000-0002-5409-3674.

Corresponding author: John Y. N. Cho, jync@ll.mit.edu

DOI: 10.1175/WCAS-D-20-0063.1

© 2020 American Meteorological Society. For information regarding reuse of this content and general copyright information, consult the AMS Copyright Policy (www.ametsoc.org/PUBSReuseLicenses).

Brought to you by NOAA Central Library | Unauthenticated | Downloaded 01/16/24 09:13 PM UTC

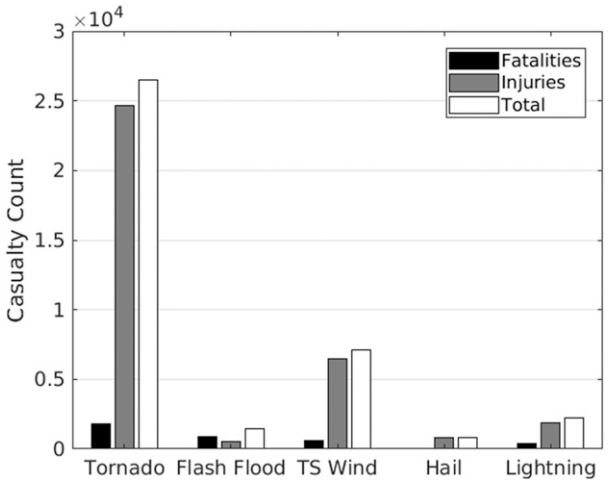

FIG. 1. Number of casualties in the United States from tornadoes, flash floods, nontornadic thunderstorm winds, hail, and lightning. The data were compiled from 1 Jan 1996 to 31 Dec 2019.

Nontornadic severe thunderstorm winds can result from a multitude of meteorological phenomena, including (but not limited to) gust fronts, microbursts, rear-flank, and forward-flank downdrafts, and rear-inflow jets in mesoscale convective systems (Doswell et al. 2005).

Figure 2 provides high-level block diagrams of the model development and usage procedures. We encourage the reader to consult these diagrams while reading the detailed explanations in section 2. Because this may be the final paper in the radar network casualty reduction benefit series for severe weather, we will conclude it by combining the models for tornadoes, flash floods, and nontornadic thunderstorm winds to give the aggregated benefit results for some basic weather radar network scenarios.

2. Model development

NWS severe weather warnings are issued to aid the public in making protection of life and property decisions (Pifer and Mogil 1978). If we can show quantitatively that 1) better radar coverage and/or performance leads to improved warning statistics, and 2) better warning performance leads to reduced casualties, then we can build a radar benefit model for casualty reduction. This is exactly what we did earlier for tornadoes (CK19a,b) and flash floods (CK20). We followed a similar methodology to develop a radar benefit model for nontornadic thunderstorm wind events.

To be consistent with the earlier models, we limited the geographic scope to the contiguous United States (CONUS). We set the start of the analysis period to be 1 January 1998, just after the completion of the Weather Surveillance Radar 1988-Doppler (WSR-88D; Crum and Alberty 1993) CONUS deployment. The end was 31 December 2019, the last date for which both storm event and storm warning data were available during the analysis. Storm event data were extracted from NOAA's National Center for Environmental Information (https://www.ncdc.noaa.gov/stormevents/), and the storm warning data were obtained from the Iowa Environmental Mesonet NWS Watch/Warnings archive (https://mesonet.agron.iastate.edu/request/gis/watchwarn.phtml).

We employed the same two radar network coverage metrics used in CK19a,b and CK20—fraction of vertical volume observed (FVO) and cross-radial horizontal resolution (CHR). FVO gives a measure of the percentage of airspace between 0 and 20 kft AGL (1 kft = 304.8 m) observed by radar while accounting for the negative effects of Earth's curvature, terrain blockage, and the radars' ''cone of silence'' (the space above the radar that is not scanned); see Fig. 1 illustration in CK19b. The reason for choosing 20 kft as the FVO ceiling is that the current radar network (on which we based the statistical analysis) has essentially perfect coverage above 20 kft, so moving the ceiling any higher would not have contributed additional information to the analysis. Details of the terrain blockage calculations are given in Cho (2015). CHR is the best horizontal resolution at a given location in a direction perpendicular to a radar's line of observation. (The horizontal resolution along the radar's line of observation is generally constant for a given radar type, so it is not useful as a coverage metric.) Maps of FVO and CHR for today's radar network are given in Figs. 2–5 in CK19a. The temporal resolution (observation update rate) is also of interest, but this will be discussed in section 2c.

There are 143 operational WSR-88Ds in the CONUS. Additionally, there are 44 CONUS Terminal Doppler Weather Radars (TDWRs; Cho and Weber 2010) operated by the Federal Aviation Administration (FAA). Figure 3 shows the radar locations. The main purpose of the TDWR is providing hazardous wind shear alerts for aircraft near airports. Their data, however, are also available to meteorologists and the public (Istok et al. 2009a). Although there is much overlap in coverage between the WSR-88D and TDWR networks, we found (via a survey of NWS offices; CK19a) that the superior vertical resolution and faster surface scan update rate of the latter have made TDWR data valuable for tornado (TOR) warning decisions. Thus, TDWRs were included in the tornado benefit model analysis.

For this study, we conducted a new survey specifically for nontornadic SVR warnings (Kurdzo and Cho 2020). We received responses from eight forecast offices (Miami, Florida; Tampa Bay, Florida; Norman, Oklahoma; Topeka, Kansas; Wilmington, Ohio; Milwaukee, Wisconsin; Charleston, West Virginia; and Peachtree City, Georgia) and the Storm Prediction Center (SPC). The responses were overwhelmingly in support of the TDWR for use in SVR warnings, especially for severe winds. One office (Topeka) claimed to have sufficient overlapping WSR-88D coverage (from KEAX and KTWX). However, all of the other respondents mentioned being aided regularly by TDWR coverage for severe weather events. As with the tornado-based survey, the Wilmington office said that given the heavy coverage from three TDWRs in their county warning area, they rely ''heavily'' on the TDWRs for SVR warnings. Another office (Milwaukee) summed up the other responses very well: ''The focus is on wind potential, as the faster scan times, lower elevation, and shorter wavelength make it very useful for microburst detection.'' With these responses in hand, as with

Brought to you by NOAA Central Library | Unauthenticated | Downloaded 01/16/24 09:13 PM UTC

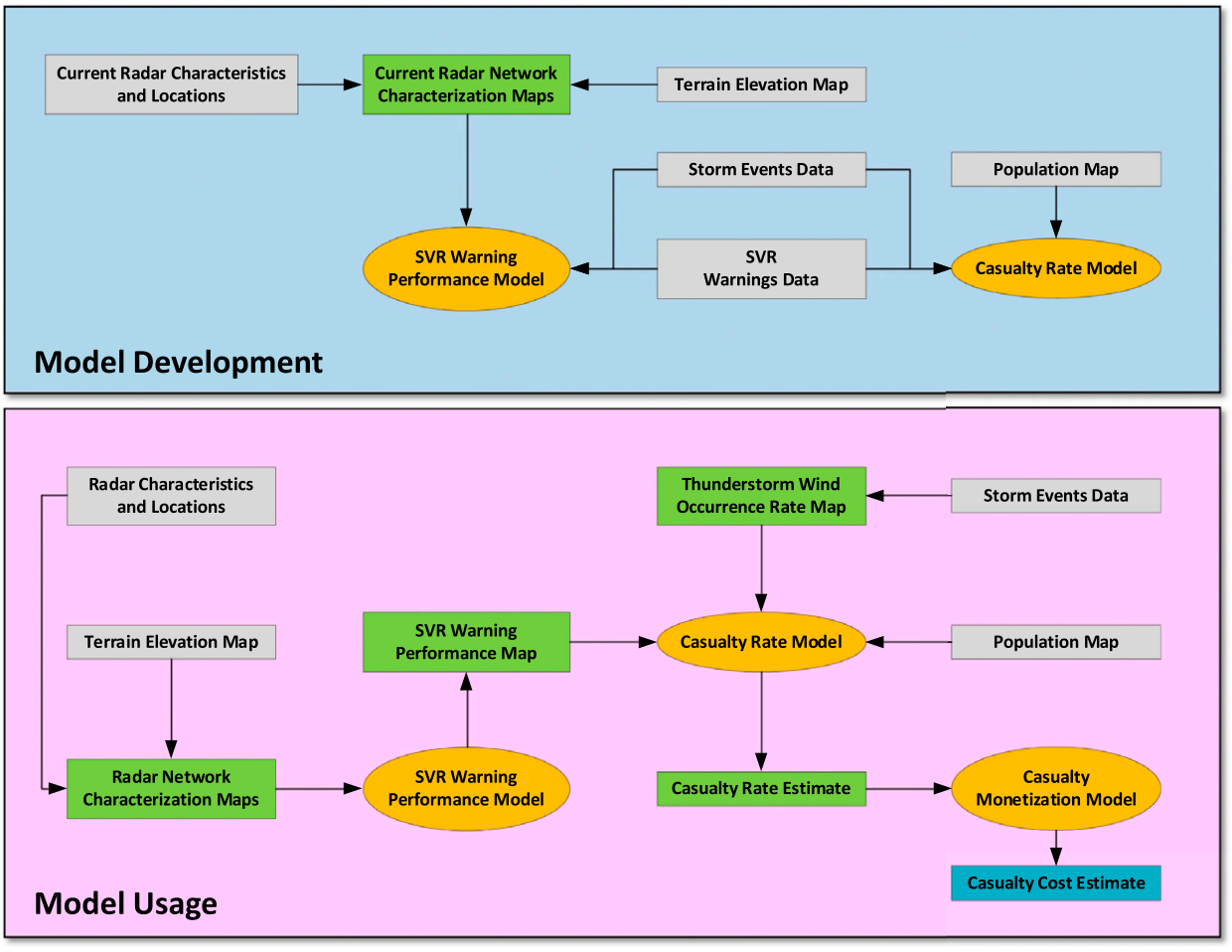

FIG. 2. (top) Development and (bottom) usage block diagrams of the radar network severe thunderstorm casualty cost model. Input data are denoted by gray rectangles, intermediate data products are shown by green rectangles, and monetized cost output is shown by a blue rectangle. Computational model components are shown as orange ovals.

the tornado-based study, we elected to include TDWRs as part of our analysis.

a. Detection probability dependence on radar coverage

Although it is generally acknowledged that weather radar is an indispensable tool in identifying SVR hazards (Burgess and Lemon 1990), as far as we know, there has not been a comprehensive study of the effects of weather radar coverage on nontornadic SVR warning performance. When the first WSR-88Ds were deployed, Polger et al. (1994) showed that the detection probability and false alarm ratio improved significantly at several individual sites when compared with the era of the predecessor radars, WSR-57 and WSR-74, which lacked Doppler capability. They analyzed three sites for dependence of detection probability, false alarm ratio, and lead time on distance from the radar, which yielded no clear trend.

For our analysis, a SVR warning was declared to be a hit if the latitude–longitude coordinates of a nontornadic thunderstorm wind or hail event were inside the warning latitude–longitude polygon, and if any part of the event time overlapped the valid warning interval; otherwise, the warning was deemed incorrect (a false alarm). This is consistent with NWS convective severe weather verification procedures (NWS 2009). In the case of a hit, the lead time was calculated to be the event start time minus the initial time of warning issuance. The detection probability was defined as the number of correct warnings (hits) divided by the number of events. The false alarm ratio was defined as the number of incorrect warnings divided by the number of warnings. Note that multiple events can occur within the time and space corresponding to a single warning, which means that even if there were no false alarms at all, the number of events will generally be greater than the number of warnings. This should be kept in mind when comparing detection probability and false alarm ratio statistics later in this section.

Next, the radar coverage metric values (FVO and CHR) were computed at the event coordinates. These data and the warning performance data were used to calculate the plots shown in the top row of Fig. 4. The FVO data were sorted based on cumulative distribution percentage intervals of [0, 1],

Brought to you by NOAA Central Library | Unauthenticated | Downloaded 01/16/24 09:13 PM UTC

FIG. 3. WSR-88D (squares) and TDWR (crosses) locations in the CONUS.

(1, 10], (10, 25], (25, 50], (50, 75], and (75, 100], while the CHR data were binned in the same but inverted order of [0, 25], (25, 50], (50, 75], (75, 90], (90, 99], and (99, 100] percentage intervals. The asymmetric interval distributions help illuminate changes in detection probability and false alarm ratio where data were sparse. The plotted abscissa values do not correspond to the middle of the data bins—instead, they are the computed actual means of the binned FVO data. The horizontal and vertical error bars denote 95% confidence intervals in both dimensions (see section 2c in CK19a for details).

SVR detection probability clearly increases with FVO and decreases with CHR. In other words, better nontornadic SVR detection performance is positively correlated with better weather radar coverage. We believe this is the first time that this link has been statistically established. However, it is possible that other factors such as storm type variation with geography and forecasting procedures specific to each weather forecast office (WFO) may work to create an apparent causal relationship between radar coverage and warning performance. To investigate this issue, we computed SVR detection probabilities for FVO values that were below and above the median FVO in each of the 117 CONUS WFOs. In ~70% of the WFOs, the detection probability was higher for the high-FVO group than for the low-FVO group, which gives credence to the CONUS-wide result. Similar results were obtained for the CHR metric. Our model does not account for WFO-specific tendencies, which must be noted as a caveat to the results in section 3.

To incorporate these relationships into our benefit model, we modeled them simply by dual-segment (“Lo” and “Hi”) linear fits with input uncertainty in both dimensions using the “fitexy” function from Press et al. (1992). The fitted results are

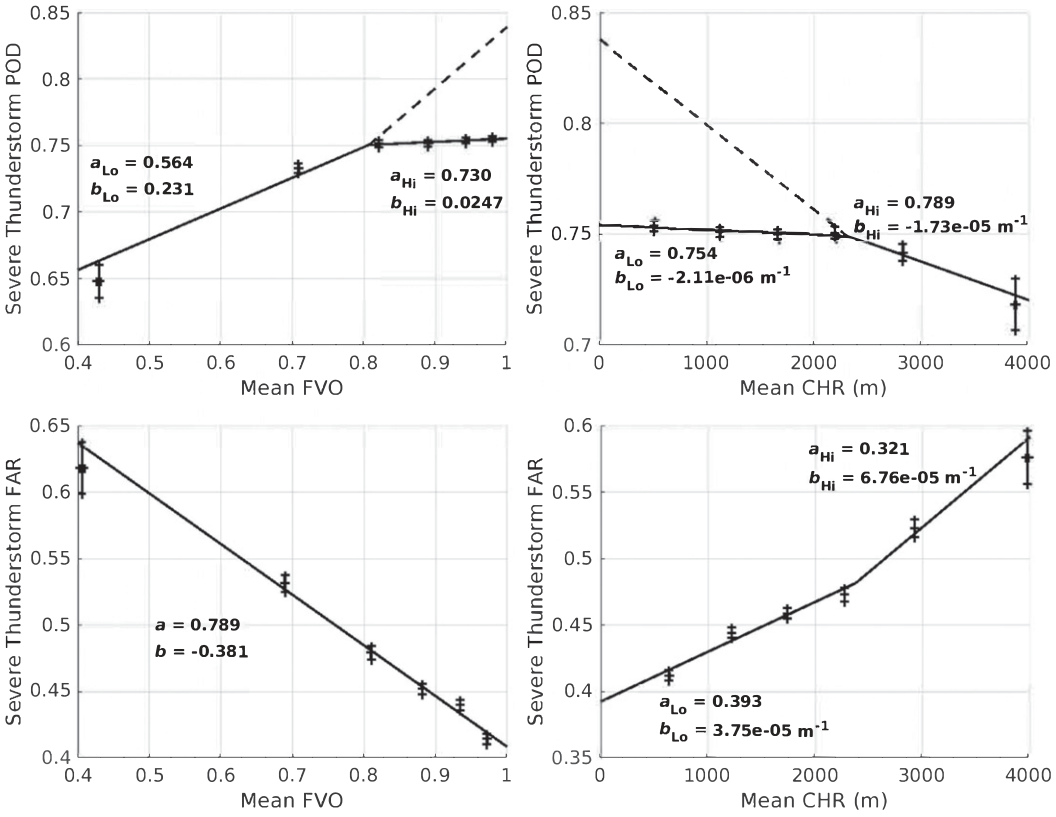

FIG. 4. Plots of (top left) SVR probability of detection vs FVO, (top right) SVR probability of detection vs CHR, (bottom left) SVR false alarm ratio vs FVO, and (bottom right) SVR false alarm ratio vs CHR. Solid lines are linear fits to the data. Dashed lines correspond to a rapid-scanning radar case.

Brought to you by NOAA Central Library | Unauthenticated | Downloaded 01/16/24 09:13 PM UTC

TABLE 1. Mean CONUS SVR detection probability and false alarm ratio.

Period	Detection probability	No. of events	False alarm ratio	No. of warnings
1 Jan 1998–31 Dec 2019 (total analysis period)	0.750 ± 0.001	579 658	0.472 ± 0.001	516 143
1 Jan 1998–30 Sep 2007 (county-based warning)	0.752 ± 0.002	248 261	0.489 ± 0.002	275 542
1 Oct 2007–31 Dec 2019 (storm-based warning)	0.749 ± 0.002	331 397	0.453 ± 0.002	240 601
1 Oct 2007–7 Mar 2011 (single polarization)	0.751 ± 0.003	90 818	0.448 ± 0.004	68 375
16 May 2013–31 Dec 2019 (dual polarization)	0.748 ± 0.002	168 613	0.466 ± 0.003	123 876

displayed in Fig. 4 as solid lines, and the ordinate intercept a and slope b values of the fitted lines are also included in the plots. (The dashed lines will be explained in section 2c.)

Event detection probability can be defined based on only positive lead times or all lead times; a negative lead time indicates that the event started before the warning issuance but was still ongoing during the warning valid period. For this study, we defined the detection probability using only positive lead times, a decision that will be explained further in section 2d. However, to examine the sensitivity of the SVR warning performance versus radar coverage relationship, we also computed detection probability statistics with all lead times. The main impact of including zero and negative lead times was to increase the overall detection probability values; however, detection probability still went up with FVO, and detection probability went down with CHR, very similar in form to the Fig. 4 plots.

To utilize both FVO and CHR relationships in the SVR detection probability model, we tried weighted additions of the two relationships. To get the optimal weights, the mean-squared sums of the difference between data and model were minimized. The optimum result was obtained with a 0.68 weight on the FVO relationship and a 0.32 weight on the CHR relationship.

Since we were able to show significant correlations between radar coverage parameters and SVR detection probability, one might also hope to find a meaningful relationship between radar coverage and warning lead time. Unfortunately, our analysis did not produce such a connection. This negative result is similar to what we found for tornadoes (CK19a).

Two major national transitions occurred during our analysis period that could affect the stability of our results. First, the NWS warning area definition changed from county-based to storm-based (e.g., Harrison and Karstens 2017) on 1 October 2007. (Sometimes the storm-based warning is referred to as polygon based.) With this change, the mean SVR warning area decreased by 35%, from 2749 to 1778 km^2, based on our data. The intent of the change was to generate more spatially precise warnings to the public. Second, the WSR-88D network was upgraded from single-polarization to dual-polarization radars (Istok et al. 2009b) between 2011 and 2013. This enhancement allows for improved discrimination of hydrometeor types such as hail, enhanced short-term forecast of storm evolution, more accurate precipitation estimates, and, in general, better data quality (e.g., Schuur et al. 2004).

We computed SVR detection probability statistics for the county-based and storm-based warning eras, then subdivided the latter between the single and dual polarization periods. For the polarization comparison, we excluded data from the intermediate interval (8 March 2011–15 May 2013) during which the CONUS WSR-88D network had a mix of both polarization types. The results (Table 1) show that detection probability was absolutely stable (at 0.75, within the indicated plus/minus 95% confidence intervals) no matter how the input data were segmented over time. (However, this also means that there was no discernible statistical benefit provided by dual polarization for this performance metric.) Based on these results, we kept the SVR detection probability versus radar coverage relationship computed for the entire 22-yr analysis period (Fig. 4, top plots).

That the SVR false alarm ratio (and the number of warnings relative to the number of events) decreased considerably after the transition to storm-based warnings is an impressive, but perhaps not unexpected, accomplishment, given the more spatially focused polygon warning areas. What is more remarkable is that the mean detection probability did not suffer (within the statistical error margins) at the same time. This may indicate that forecasters generally had the skill to forecast SVR events to better than the county boundary resolution (especially for large counties) even before the official transition date.

b. *False alarm ratio dependence on radar coverage*

Unlike the SVR detection probability statistics, the false alarm ratio changed over the course of the analysis period (Table 1). There was meaningful reduction in the false alarm ratio after the transition from county-based to storm-based warning, which is similar to our TOR warning false alarm ratio results (Tables 2 and 3 in CK19a). The SVR warning false alarm ratio within the storm-based warning era, however, increased after the switch to dual polarization WSR-88Ds, which is disappointing. There were likely other factors besides the change in radar polarization that contributed to the rise in false alarm ratio, but that is beyond the scope of this study.

In terms of the false alarm ratio versus radar coverage model development, we decided to use data from the entire storm-based warning period as a compromise between temporal stability of overall false alarm ratio and error reduction of the binned means. The resulting plots are shown in Fig. 4 (bottom row). The SVR warning false alarm ratio unambiguously decreases with FVO and increases with CHR. As with detection probability, better SVR warning false alarm ratio performance correlates positively with better weather radar coverage. Again, we believe this is the first time that this link has been statistically established. However, as is the case with detection probability, it is possible that other factors may work to create

Brought to you by NOAA Central Library | Unauthenticated | Downloaded 01/16/24 09:13 PM UTC

an apparent causal relationship between radar coverage and false alarm performance. To probe this issue, we computed SVR false alarm ratios for FVO values that were below and above the median FVO in every CONUS WFO. In ~80% of the WFOs, the false alarm ratio was lower for the high-FVO group than for the low-FVO group, which supports the CONUS-wide result. Similar results were obtained for the CHR metric.

To generate the modeled relationships, the false alarm ratio versus FVO data were fit to a single line, while the false alarm ratio versus CHR data were fit to two linear segments (''Lo'' and ''Hi''); the y intercept a and slope b values of the fitted lines are displayed in the Fig. 4 plots.

To incorporate both FVO and CHR relationships in the SVR warning false alarm ratio model, we tried weighted additions of the two relationships. To achieve the optimal weights, the mean-squared sums of the difference between data and model were minimized. The best result was obtained with a 0.44 weight on the FVO relationship and a 0.56 weight on the CHR relationship.

Note that we analyzed SVR detection probability and false alarm ratio separately, even though they are interdependent in reality. The warning performance goal is a detection probability of 1 and a false alarm ratio of 0, which is impossible to achieve operationally—in general, pushing to raise the detection probability tends to also increase the false alarm ratio, and lowering the false alarm ratio without dragging down the detection probability is likewise difficult. To take this dependence into account, combined statistical metrics such as the critical success index (CSI) have been touted for warning performance measurement and optimization (e.g., Brooks and Correia 2018). We did not, however, adopt this approach because of two reasons: 1) Although detection probability (via absence/presence of warning) could be tested as a predictor in the casualty regression model on a per-event basis (section 2d), false alarm ratio and CSI could not. 2) To create a geospatial map of historical warning performance for use by the regression model, the footprint mismatch between detection probability (event coordinates) and false alarm ratio (warning polygons) calculations posed a problem in combining them for CSI.

c. *Rapid-scan effects*

Meteorological radar scan update rate is limited by the need to collect enough samples over a given location to reduce measurement error and enhance ground clutter filtering; it is also constrained by the mechanical pointing performance of the antenna. WSR-88D volume coverage patterns (VCPs) for convective weather have periods of 4.5 to 6 min, while TDWR hazard mode scans have ~2.5-min volume update periods (with sparse elevation-angle sampling) and a 1-min period for surface scans. Since 2011, adaptive VCP modifications have been introduced to the WSR-88Ds that selectively skip the highest elevation angle cuts or inserts more frequent low-level cuts based on storm morphology (Chrisman 2013, 2014, 2016), but volume update rates are still ultimately limited by the radar parameters. We are currently analyzing the effects of these adaptive scan patterns with variable scan update periods on severe weather warning performance and expect to publish the results in a future paper.

Substantially faster update rates may be possible in the future by operational deployment of electronically scanned phased array radars (e.g., Weber et al. 2007, 2017; Heinselman et al. 2008). Since our aim is to apply our model to potential future radar networks, we need to quantify any additional benefits accrued via rapid scanning.

The National Weather Radar Test bed (NWRT; Heinselman and Torres 2011) was utilized in phased array radar innovative sensing experiments (PARISE) to analyze the impact of faster observational updates on the decision-making process of weather forecasters. Three storm categories (squall line, supercell cluster, and supercell) were analyzed during the 2015 PARISE (Wilson et al. 2017), with scan update periods of 61–76 s. The radar data were sampled at different intervals to output full- (~1 min), half- (~2 min), and quarter- (~5 min) speed data. Each time-resolution dataset was provided to a different group of 10 NWS forecasters for SVR and TOR warning guidance. The quarter-speed case is reflective of most of the meteorological radar data employed in our regression study, so that was considered to be our baseline.

Figure 5 in Wilson et al. (2017) gives the event-specific SVR warning results. Over the three storms studied, there were two thunderstorm wind and three hail events. As our model only includes the former, we took the average over the thunderstorm wind events (the beta case and one of the delta events, marked by red in this figure). In both cases, the full-speed thunderstorm wind detection probability was 1. At quarter speed, the detection probability was 0.8 for the beta case and 1 for the relevant delta event, which yielded an average detection probability of 0.9. The full-speed SVR warning false alarm ratio, however, showed no improvement over the quarter-speed false alarm ratio. Thus, we developed a rapid-scan version of the detection probability versus radar coverage model, but not for false alarm ratio versus radar coverage.

Since the rapid-scan analysis was based on a small sample size, we applied the results conservatively. The 2015 PARISE was carried out over good radar coverage, so with respect to the top-row plots of Fig. 4, we only considered altering the detection probability versus FVO relationship at high FVO values, and the detection probability versus CHR curve at low CHR values. For rapid-scan radars (i.e., for 1-min update scans), we enhanced the detection probability versus FVO relationship as indicated by the dashed line in the top left plot of Fig. 4. The rapid-scan detection probability value at FVO = 1 is given by 1/0.9 (the detection probability improvement ratio seen in PARISE) times the baseline-speed detection probability at FVO = 1. In the same way, we increased the detection probability versus CHR line for the rapid-scan case as denoted by the dashed line in the top right plot of Fig. 4.

We can also obtain the median SVR warning lead times for different scan speeds from Fig. 5 in Wilson et al. (2017). For the two thunderstorm wind cases, the full-speed median lead times were 19.5 min (beta case) and 22.5 min (delta case), giving an average of 20.5 min. The quarter-speed median lead times were 10.5 min (beta) and 24.5 min (delta), yielding an average of

Brought to you by NOAA Central Library | Unauthenticated | Downloaded 01/16/24 09:13 PM UTC

17 min. Thus, on average for the thunderstorm wind cases, the SVR warning lead time increased by 20.5–17 = 3.5 min from the baseline to the full-speed case. However, in the delta case, the full-speed lead time was actually less than the quarter-speed lead time. Given these mixed results, we decided to take the conservative approach and not attribute any lead time gain to rapid scanning.

In contrast to other components of our benefit model that were developed using many years of historical data, the rapid-scan impacts discussed above were based on one experimental campaign. Therefore, the resulting rapid-scan-related benefits should be taken with some caution. Further studies on the impact of scan speed on severe weather warning performance are needed to provide a more statistically robust input to our benefit model.

d. Casualty dependence on severe thunderstorm warning

With statistical links between radar coverage and SVR warning performance established, we go on to discuss the potential link between SVR warnings and casualty rates. SVR warning can be verified by reports of thunderstorm wind or hail events, so we took the casualties due to these two event types separately for the regression analysis.

While the public's response to TOR warnings has been studied extensively (e.g., Simmons and Sutter 2011), and we know that warnings do have a role in reducing tornado casualties (e.g., CK19a), the picture with nontornadic severe storm warnings is less clear (Black and Ashley 2011). Whereas there is definitive guidance on what to do when a TOR warning is issued (take shelter), people's response to a SVR warning may be more varied and context dependent. For example, those already inside a building may do nothing, those that are walking or biking outside may seek shelter, and those that are in vehicles may or may not continue driving. With the perception that a SVR warning represents less of a threat to life than a TOR warning, we might expect, a priori, to find a more ambiguous relationship between SVR warning performance and casualty rate.

In our regression analysis, casualties were not separated into fatalities and injuries. Since the vast majority of events have zero casualty, raising the number of nonzero outcomes by grouping fatalities and injuries together improves statistical robustness. Also, while the storm database tabulates direct and indirect casualties separately, we only counted direct casualties in our study, because we wanted the tightest causal link between the events and their impact on people. The casualty model results are later separated into fatalities and two kinds of injuries in the monetization stage (section 2e) based on historical averages.

The casualty variances were 11 and 26 times higher than the casualty means over our analysis period for nontornadic thunderstorm wind and hail events, respectively. Therefore, instead of a Poisson distribution that is used for counting statistics when the outcome variance and mean are similar, we assumed a more general negative binomial distribution model for the casualty count,

$$C \sim \text{NegBin}(\mu, \theta), \tag{1}$$

for our regression analysis, where μ is the distribution mean and θ is the dispersion parameter (e.g., Simmons and Sutter 2008). A linear combination of predictor variables set equal to $\ln \mu$ then becomes the casualty regression model. The same scheme was used in the tornado (CK19a,b) and flash flood (CK20) studies.

We employed the "glm.nb" function from the open software package R (https://www.R-project.org/) for the negative binomial regression analysis. First, we tried the absence/presence (0/1) of warning as a predictor variable before progressing to combinations of multiple factors. The results showed that casualties due to hail had no statistical correlation with the presence of SVR warning. Subsequently, we tried different combinations of predictor variables, including warning lead time, but we did not see the probability of the null hypothesis being true fall below the typically used threshold of 0.05 for warning presence or warning lead time. Therefore, we abandoned reduction of hail casualties as a potential benefit for weather radars and concentrated solely on nontornadic thunderstorm wind casualties. This omission should not affect the model results much, because hail has not produced any reported fatalities in the CONUS over our study period, and injury rates were very low (Fig. 1).

Past studies of nontornadic convective wind casualties have focused on fatalities (e.g., Ashley and Black 2008). Since a fatality can be considered as the extreme end of a casualty continuum that also spans injuries, we can start by drawing on the work that others have already done on fatality causes.

We only considered casualty impact factors that could be geospatially quantified, in keeping with the goals of the radar network benefit study. Although temporal trends (seasonal, time of day) have been observed (Black and Ashley 2010), we did not regard them as relevant to our time-independent cost model. Felled-tree fatalities were dominant, and, of these, most victims were outdoors or in vehicles, rather than inside buildings (Schmidlin 2009). Unlike the tornado case, few thunderstorm wind fatalities occurred in mobile housing, while boating accidents—rare for tornadoes—were a notable source of deaths (Black and Ashley 2010). (Since we had the fraction of population in mobile housing geospatial data from our tornado study, we tried it as a casualty predictor, but it had no statistically meaningful relationship with casualty rate in this case.)

The National Centers for Environmental Information (NCEI) storm database has sparse coverage of aviation casualties. This was a concern for the era before the mid-1990s when commercial airline accidents due to microbursts accounted for a significant fraction of nontornadic thunderstorm wind fatalities (Black and Ashley 2010). Since then, however, this class of incidents has virtually vanished in the United States as a result of the deployment of various wind shear detection systems (ground-based and on board), as well as from improved pilot training. Hallowell and Cho (2010) monetized the benefits provided by these systems (which includes the TDWR) via aviation-specific wind shear alerts. Our current study, dealing solely with NWS severe weather warnings, excludes benefits from those aviation-specific alerts. Because of the effectiveness of the wind shear detection systems, commercial aircraft

Brought to you by NOAA Central Library | Unauthenticated | Downloaded 01/16/24 09:13 PM UTC

FIG. 5. Mean annual nontornadic thunderstorm wind casualty density.

casualties due to convective wind shear should continue to be negligible in the United States, provided that the current wind shear detection systems remain in place or are replaced by equivalent or better systems. As for general aviation accidents, convective weather is listed as a contributing cause in only 3% of fatalities for the period spanning 1982–2013 (Fultz and Ashley 2016).

The spatial pattern of nontornadic thunderstorm wind casualties for our analysis period (1998–2019) is shown in Fig. 5. Casualties were accumulated for each cell in the 1/120° × 1/120° latitude–longitude model grid (about 900-m spacing at midlatitudes). As this raw representation would not show up visually at CONUS scale, the sums were then smoothed with a 2D Gaussian kernel with a width of 1/12°, and then divided by the number of years to get the annual casualty rate density. There is a general correlation with population density (e.g., Figs. 2–14 in CK19a), which is unsurprising. Population centers on the West Coast are the exception, which is likely due to the scarcity of thunderstorm occurrence in that region. At this scale, there is no obvious correlation with bodies of water or forest cover (e.g., Fig. 8c in Ashley 2007)—these may become apparent at very finescale, but lacking fidelity in spatial coordinates (all casualties per event are generally recorded as one location, for example) and not having a national database pinpointing tree locations, we were left with population density as our main predictor candidate, besides the measures of SVR warning performance.

Thus, the independent variables that we tried in the casualty regression analysis were 1) logarithm of the population density, 2) historical SVR warning false alarm ratio, 3) SVR warning lead time, and 4) presence of SVR warning. The historical false alarm ratio was considered, because it yielded useful results in our tornado analysis (CK19a,b), possibly because of the "cry wolf" phenomenon (e.g., LeClerc and Joslyn 2015). Since the switch from county- to storm-based warning in October 2007 made a noticeable difference in false alarm ratio statistics, we generated two temporally averaged false alarm maps (1 January 1998–30 September 2007 and 1 October 2007–31 December 2019) to be applied to the regression analysis for events before and after the transition, respectively (Fig. 6).

The population density data were obtained from the Center for International Earth Science Information Network (CIESIN 2017) with grid spacing that matched our 1/120° × 1/120° latitude–longitude model resolution. Measured density for 2005, 2010, and 2015 were available as well as projected data for 2020; linear interpolation produced corresponding data for the other years.

Following CK19a, we combined warning lead time (see Fig. 7 for histogram) and absence/presence of warning into one variable, because keeping each as a separate independent variable degraded the overall regression statistics (likely because they are tightly coupled in reality). To do this, we defined the presence of a warning (as related to detection probability statistics) to be restricted to lead times with positive values only. In this way, the warning lead time variable completely encompassed the absence/presence of a warning, where 0 is absence and any positive value is presence.

The resulting regression equation is

$$\ln \mu = \alpha \ln D + \beta F + \gamma T + k, \tag{2}$$

where D is the population density (km^{-2}); F is the historical false alarm ratio; T is the lead time (s); k is the intercept constant; and α, β, and γ are the regression coefficients. The fitted parameter results are given in Table 2. All coefficient estimates had the expected signs, that is, casualty per nontornadic thunderstorm wind event was positively correlated with local population density and historical false alarm ratio, and it was negatively correlated with SVR warning lead time. The coefficient signs do not flip within the standard errors, and the z statistics (Wald test) showed that all parameter estimates were significant at a better than 7×10^{-6} level. (The z value is the parameter estimate divided by its standard error, and the probability of exceeding $|z|$ is rejection of the null hypothesis at that

Brought to you by NOAA Central Library | Unauthenticated | Downloaded 01/16/24 09:13 PM UTC

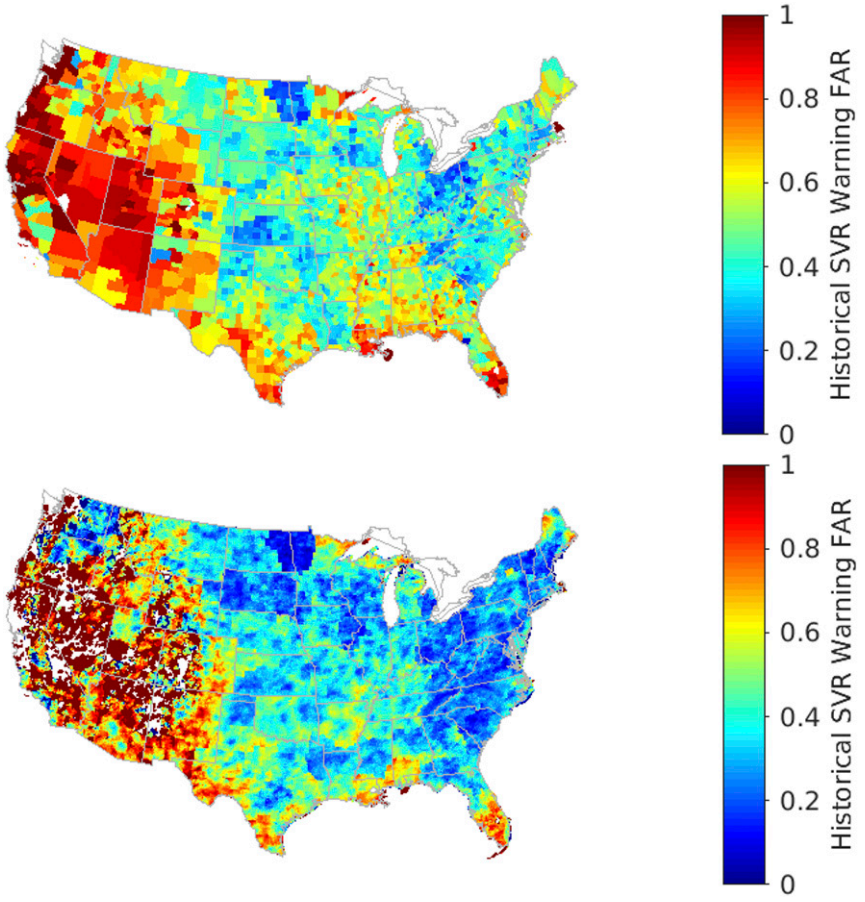

FIG. 6. Historical SVR warning false alarm ratio (top) from 1 Jan 1998 to 30 Sep 2007, in the county-based warning era, and (bottom) from 1 Oct 2007 to 31 Dec 2019, in the storm-based warning era. White indicates areas with no SVR warning issued during the respective period.

level.) Furthermore, every variable was a statistically significant predictor of casualty rate, according to degree-of-freedom chi-square tests. This was a key result—the first, that we are aware of, showing hard evidence for better SVR warning performance leading to reduced nontornadic thunderstorm wind casualties.

Application of Eq. (2) with the fitted parameters in Table 2 and the actual median lead time for nontornadic thunderstorm wind events (1200 s) to the same input data resulted in a casualty count of 6295 as compared with the actual count of 6266, which is only a 0.5% difference. According to this model, the presence of a SVR warning with the 1200-s median lead time reduces nontornadic thunderstorm wind casualty by 14% relative to no warning (zero lead time).

e. Casualty monetization

Reliance on value of a statistical life (VSL) is standard practice for monetizing casualties in the actuarial world. As we did earlier (CK19a,b; CK20), we followed the Department of Transportation (DOT 2016) guideline, which established a VSL of $9.6 million (M) in 2015 dollars. (This valuation is specific to the United States. Other developed nations have different casualty cost standards.) To update the value to 2020 dollars, we used their equation,

$$\mathrm{VSL}_T = \mathrm{VSL}_0 \frac{\mathrm{CPI}_T}{\mathrm{CPI}_0} \left(\frac{\mathrm{MUWE}_T}{\mathrm{MUWE}_0} \right)^q, \tag{3}$$

where CPI is the consumer price index, MUWE is the median usual weekly earnings, q is income elasticity, and subscripts T and 0 correspond to updated base year and original base year. We extracted $\mathrm{CPI}_T/\mathrm{CPI}_0 = 1.10$ (https://www.bls.gov/data/inflation_calculator.htm) and $\mathrm{MUWE}_T/\mathrm{MUWE}_0 = 1.18$ (https://www.bls.gov/cps/cpswktabs.htm) from the U.S. Bureau of Labor Statistics database, for a baseline time of January 2015 and updated month of January 2020. We obtained a 2020 VSL of $12.5M using the DOT's recommended value of $q = 1$.

As discussed in section 2d, we did not distinguish between fatalities and injuries in our casualty regression model. Instead, we took the actual fatality and injury statistics computed over the analysis period to separate the model output into the two casualty types, which yielded 9% fatalities and 91% injuries.

Injuries were monetized as fractions of VSL following Table 3 in DOT (2016), which gives the fractional VSL based

Brought to you by NOAA Central Library | Unauthenticated | Downloaded 01/16/24 09:13 PM UTC

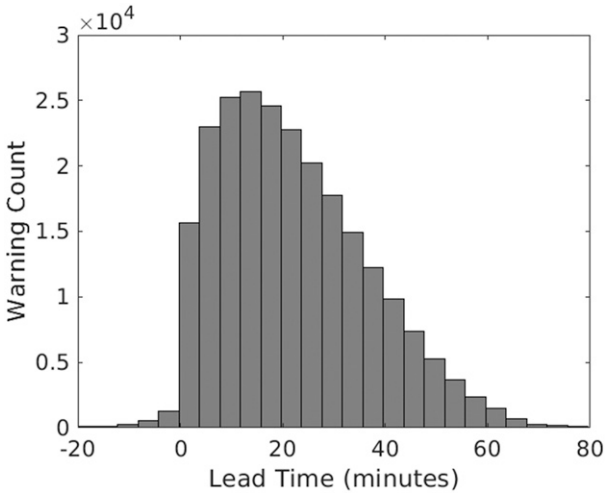

FIG. 7. Histogram of SVR warning lead times for nontornadic thunderstorm wind events. The median lead time is 1200 s (20 min), regardless of whether negative lead times are included.

on injury level. However, because injury levels were not mapped to the hospitalized versus treated–released categories in the DOT document, we followed Tables 14 and 15 in FEMA (2009) that assign hospitalization cases to level 4 and treated–released cases to level-2 injuries. Since level-4 and level-2 injury costs are set at 0.266 × VSL and 0.047 × VSL, respectively, in DOT (2016), we arrived at per-injury costs of 0.266 × \$12.5M = \$3.33M (hospitalized) and 0.047 × \$12.5M = \$0.588M (treated–released) in 2020 dollars. Note that there are other VSL and injury cost valuation procedures; we simply selected the most recent one issued by the federal government that we could find.

The storm event database does not report injuries by severity. To obtain a reasonable estimate of the mean ratio of hospitalized to released cases, we consulted a compendium of wind-storm-induced casualty studies (Goldman et al. 2014). There we found five relevant (nontornadic) studies covering a total of 2587 injuries. The median percentages overall were 10% for injuries requiring hospitalization and 90% for injury cases that were treated and released, which we adopted for our model.

f. Geospatial grid computation

The model components can now be assembled to produce mean annual CONUS nontornadic thunderstorm wind casualty cost. The modeled casualty rate (per year, per grid cell) is expressed as

$$R_{ij}^{F,H,R} = Y^{F,H,R}[r_{ij}(1)B_{ij} + r_{ij}(0)(1 - B_{ij})]O_{ij}, \tag{4}$$

where B is the warning probability (i.e., detection probability) per nontornadic thunderstorm wind event, O is the nontornadic thunderstorm wind occurrence rate, i and j are the latitude and longitude grid indices, and the superscripts connote fatal (F), injured—hospitalized (H), and injured—treated and released (R). The latitude–longitude grid spacing is 1/120°. The casualty class fractions are subdivided as

$$Y^F = f, \tag{5}$$

$$Y^H = (1 - f)h, \quad \text{and} \tag{6}$$

$$Y^R = (1 - f)(1 - h), \tag{7}$$

where f is the fatality fraction and h is the fraction of hospitalized injuries. From Eq. (2) we derive the casualty rate per event,

$$r_{ij}(W) = \exp[\alpha \ln(P_{ij}) + \beta F_{ij} + \gamma T + k], \tag{8}$$

with ($W = 1$) and without ($W = 0$) a SVR warning. The lead time variable T is set to 0 when W is 0. When W is 1, T is set to the historical median value (1200 s). If future experiments show convincingly that faster radar scanning increases median SVR warning lead time, then T can be set to an appropriately higher value for the rapid-scan case.

The gridded warning probability B_{ij} in Eq. (4) is generated by applying the Fig. 4 (top panels) fitted parameters to the radar network FVO and CHR maps, then combining the two with the optimized weights given in section 2a. The gridded false alarm ratio F_{ij} in Eq. (8) is produced by applying the Fig. 4 (bottom panels) fitted parameters to the radar network FVO and CHR maps, then summing the two with the optimal weights given in section 2b.

For the gridded nontornadic thunderstorm wind occurrence rate O_{ij} in Eq. (4), events over the analysis period were accumulated in the 1/120° × 1/120° model grid. The sums were smoothed with a 0.75° 2D Gaussian kernel, then divided by the number of years to get the mean annual occurrence rate per grid cell; Fig. 8 shows the result as a spatial density map. The smoothing is needed to dissipate the artificial tendency of nontornadic thunderstorm wind occurrence reports to cluster around population centers (Doswell et al. 2005). Admittedly, the degree of smoothing applied is somewhat subjective, based on the perceived balance between actual occurrence inhomogeneity and observational bias. We tried to eliminate cases of overreporting by rejecting events in a given grid cell that overlapped in time with an earlier event.

TABLE 2. Nontornadic thunderstorm wind casualty model regression results.

Fitted coef/parameter	Estimate	Std error	z	Pr (>|z|)
α (log population density)	0.156	0.0108	14.4	$<2 \times 10^{-16}$
β (historical false alarm ratio)	1.45	0.176	8.25	$<2 \times 10^{-16}$
γ (warning lead time)	-1.24×10^{-4}	2.78×10^{-5}	−4.48	7×10^{-6}
k (intercept constant)	−5.00	0.0934	−53.5	$<2 \times 10^{-16}$
θ (dispersion parameter)	6.54×10^{-3}	1.83×10^{-4}	—	—

Brought to you by NOAA Central Library | Unauthenticated | Downloaded 01/16/24 09:13 PM UTC

FIG. 8. Mean annual nontornadic thunderstorm wind occurrence rate density.

The CONUS nontornadic thunderstorm wind casualty rate parsed by casualty type is computed by summing Eq. (4) over all grid indices. The total annual CONUS casualty cost is generated by multiplying the individual casualty rates with the corresponding casualty category costs (cf. section 2e) and summing.

3. Example results

We computed the modeled nontornadic thunderstorm wind casualty costs for five CONUS radar network configurations: 1) no radar coverage, 2) current network (WSR-88Ds and TDWRs), 3) current network enhanced with rapid-scan capability (one-minute volume updates), 4) perfect radar coverage with WSR-88D-like resolution and scan performance, and 5) perfect radar coverage with rapid-scan capability. ''Perfect radar coverage'' was defined by letting FVO = 1 and CHR = 0 everywhere. For the ''no radar coverage'' case, we set FVO to 0 and CHR to the 99th percentile value (4270 m) everywhere. Note that this differs from how we defined ''no radar coverage'' previously, where CHR was set to infinity (CK19a,b; CK20). The reason for this change is that the detection probability and false alarm ratio versus CHR curves (Fig. 3, right-hand plots) do not reach asymptotes with increasing CHR as they did in the tornado and flash flood cases. Thus, to keep the results within physically reasonable bounds but at the same time reflective of nonexistent coverage, we chose the 99th-percentile CHR value.

Table 3 lists the nontornadic thunderstorm wind casualty estimates for all scenarios, and the actual average annual casualty rates. There is excellent agreement between the baseline (current radar network) model results and the actual average casualty rates, especially for the actual median casualty rates. Figure 9 displays the modeled baseline casualty rate density over the CONUS. Although more spatially diffuse compared to the historical casualty rate map (Fig. 5), which is to be expected, the general patterns are quite similar, which gives us more confidence that our geospatial cost model is behaving reasonably.

Table 4 gives the corresponding nontornadic thunderstorm wind casualty costs. All costs are in 2020 dollars. Compared to a CONUS without weather radars, the current baseline provides about \$200M yr^{-1} in nontornadic thunderstorm wind casualty reduction benefits. The remaining benefit pool is modest—about \$36M yr^{-1} for perfect radar coverage with rapid-scan capability.

Figure 10 shows the geospatial pattern of the remaining benefit pool for nontornadic thunderstorm wind casualties.

TABLE 3. Annual CONUS nontornadic thunderstorm wind casualty estimates. Actual average injured counts are totals and are not broken out by injury type.

Scenario	Fatal	Injured (hospitalized)	Injured (treated and released)	Total	Delta baseline
No radar coverage	31	32	287	350	109
Current radar coverage	22	22	197	241	—
Current radar coverage, rapid scan	21	22	196	239	−2
Perfect coverage	20	21	184	225	−16
Perfect coverage, rapid scan	20	20	182	222	−19
Actual median (1998–2019)	22 ± 2		239 ± 18	259 ± 19	—
Actual mean (1998–2019)	25 ± 3		259 ± 31	285 ± 32	—

Brought to you by NOAA Central Library | Unauthenticated | Downloaded 01/16/24 09:13 PM UTC

FIG. 9. Modeled mean annual nontornadic thunderstorm wind casualty rate density for the current weather radar network.

The background honeycomb-like imprint in the eastern CONUS corresponds to the low-altitude coverage pattern of the current weather radar network. The largest benefits remain in Appalachian Mountain regions where terrain blockage is an issue for low-level radar coverage, and where population density and nontornadic thunderstorm wind occurrence rates are relatively high. We refer the reader to our previous papers for analogous benefit pool maps for tornadoes (Fig. 3-4 in CK19a) and flash floods (Fig. 9 in CK20).

In summary, Table 5 lists the estimated annual CONUS costs due to tornadoes, flash floods, and nontornadic thunderstorm winds in 2020 dollars. Costs for the former two were updated to reflect January 2020 employment, earnings, and VSL figures. The tornado costs include sheltering costs in addition to casualty costs (CK19a). Both costs and benefits are dominated by tornadoes, which is not surprising given their large share of the casualty count (Fig. 1). In terms of the benefits that the current radar network provides, however, the contribution of flash flood and nontornadic thunderstorm wind casualty reduction is significant, nearly doubling the benefit from \$575M yr^{-1} for tornadoes only to just over \$1.1 billion (B) yr^{-1} in total. The remaining benefit pool, on the other hand, is overwhelmingly provided by tornado cost reduction. These observations are highlighted graphically in Fig. 11.

We note several cautionary points about our benefit model. First, severe weather warnings are issued by forecasters, not radar-based algorithms, so performance will depend on other inputs as well as human factors (Andra et al. 2002), including cultural tendencies peculiar to each WFO (Smith 2011). One can perhaps see effects of the latter in the historical SVR false alarm ratio maps (Fig. 6), where there are discontinuities in false alarm ratio along lines that often coincide with NWS county warning area boundaries. But our model does not attempt to characterize and quantify all such influences on SVR warning performance.

Second, severe weather event records are imperfect; thunderstorm wind occurrence data for warning verification are notably so (e.g., Witt et al. 1998; Trapp et al. 2006). As mentioned already in section 2f, there is likely a reporting bias toward population centers, and the spatial extent of each event is only characterized by one or two coordinates.

Third, the radar volume rapid-scan effects were modeled based on only a small number of experiments. In response, we took a cautious approach, including only the consistent effect observed on detection probability. It is possible that additional rapid-scan benefits due to lead time and false alarm ratio improvements would be uncovered if further experiments are performed. We therefore advocate collecting more statistics on the impact of faster volume scans on SVR warning performance by using existing and new radars capable of finer temporal resolution observations (e.g., Kurdzo et al. 2017; Hondl and Weber 2019) compared to the current operational radars. In the future, the added use of rapidly observed polarimetric signatures of storm development, such as differential reflectivity

TABLE 4. Annual CONUS nontornadic thunderstorm wind casualty cost estimates (millions of dollars).

Scenario	Fatal	Injured (hospitalized)	Injured (treated and released)	Total	Delta baseline
No radar coverage	391	106	168	665	207
Current radar coverage	269	73	116	458	—
Current radar coverage, rapid scan	267	72	115	454	−4
Perfect coverage	251	68	109	428	−30
Perfect coverage, rapid scan	248	67	107	422	−36

Brought to you by NOAA Central Library | Unauthenticated | Downloaded 01/16/24 09:13 PM UTC

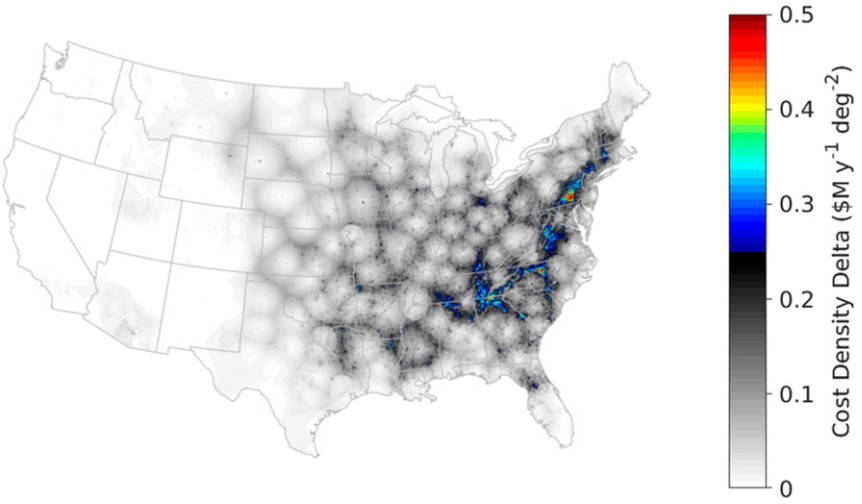

FIG. 10. Difference in modeled mean annual nontornadic thunderstorm wind casualty cost density between the perfect radar coverage with rapid-scan case and the baseline (current radar network) case.

columns, may also improve SVR warning performance (Kuster et al. 2019).

Fourth, the multiple factors inducing thunderstorm wind casualties are complex and hard to model. As discussed in section 2d, the majority of U.S. fatalities occur while the victim is outdoors, in vehicles or in boats, which cannot be precisely characterized by population density data. Also, it is difficult to geospatially quantify factors like real-time access to SVR warnings, likelihood and form of response, and vulnerability (e.g., Black and Ashley 2011).

Fifth, we had a relatively small number of data points on which to base the SVR warning performance model under near-zero radar coverage conditions. Therefore, the ''no radar coverage'' results in Tables 3–5 must be viewed with some caution.

Despite these caveats, we posit that the simplifications and approximations employed in constructing our geospatial benefit model were, to a large extent, compensated for by the sheer volume (hundreds of thousands) of data points (Table 1) used in the analysis. Errors and uncertainties tend to get averaged out over many instances. The resulting statistical robustness would not be achievable in a more detailed case-study approach (which would still be complementary and insightful as well).

4. Summary discussion

Via statistical geospatial analyses on historical CONUS data (1998–2019), we showed, likely for the first time, that better weather radar coverage is meaningfully correlated with higher detection probability and lower false alarm ratio for nontornadic SVR warnings. Furthermore, also perhaps for the first time, we established that improved SVR warning performance (presence of warning, increased lead time, and lower historical false alarm ratio) is statistically linked to reduced nontornadic thunderstorm wind casualty rates. These results are similar to what we found for tornadoes (CK19a,b) and flash floods (CK20). We combined these statistical relationships to form a geospatial econometric model for estimating nontornadic thunderstorm wind casualty costs for a given meteorological radar network. The difference between the casualty cost for a particular configuration and a baseline network yielded the benefit.

The model showed that today's CONUS weather radar network provides about \$200M yr^{-1} in benefits with respect to nontornadic thunderstorm wind casualty cost reduction. The remaining benefit pool was modest, with \$36M yr^{-1} for perfect radar coverage with rapid-scan capability.

Aggregating these results with those for tornado and flash flood benefits, we got a total of just over \$1.1B yr^{-1} benefit for the current CONUS radars. The combined remaining benefit

TABLE 5. Annual CONUS severe storm cost estimates (millions of dollars).

Scenario	TOR	TOR delta baseline	FF	FF delta baseline	SVR wind	SVR wind delta baseline	Total	Total delta baseline
No radar coverage	4192	575	1058	341	665	207	5915	1123
Current radar coverage	3617	—	717	—	458	—	4792	—
Current radar coverage, rapid scan	3259	−358	717	0	454	−4	4430	−362
Perfect coverage	3421	−196	702	−15	428	−30	4551	−241
Perfect coverage, rapid scan	2890	−727	702	−15	422	−36	4014	−778

Brought to you by NOAA Central Library | Unauthenticated | Downloaded 01/16/24 09:13 PM UTC

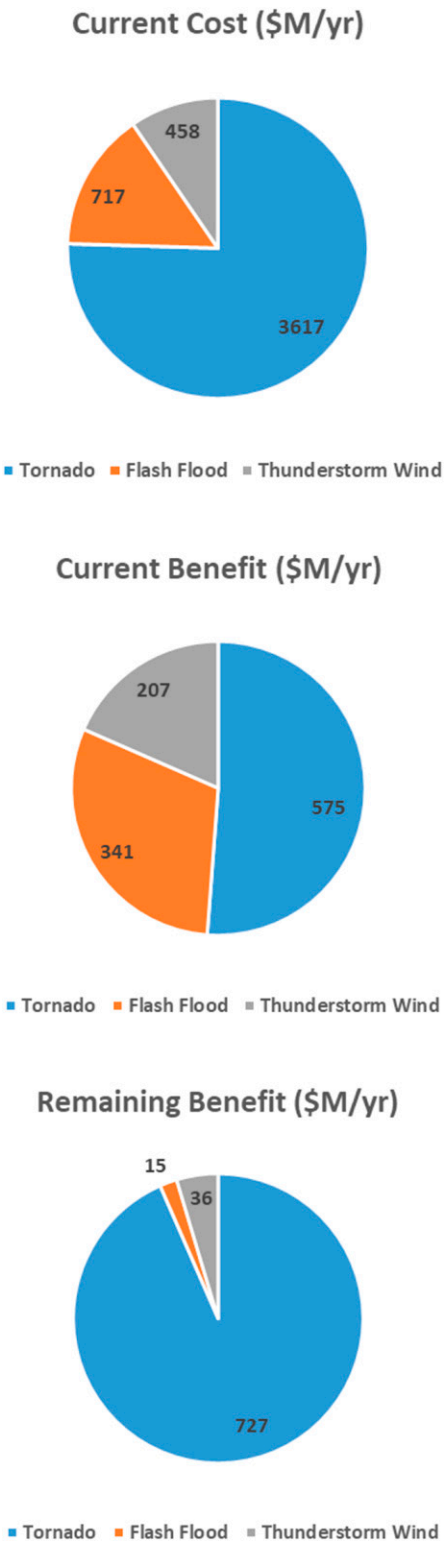

FIG. 11. Modeled relative contributions of tornado, flash flood, and nontornadic thunderstorm wind in the CONUS to (top) mean annual cost, (middle) annual benefit provided by the current radar network, and (bottom) remaining annual benefit pool that would be given by perfect radar coverage and rapid-scan capability.

for enhanced coverage and scan update rate was estimated to be about \$780M yr^{-1}.

An interesting collateral result that came out of our historical data analysis is that after the transition from county-based to storm-based SVR warnings on 1 October 2007, the mean false alarm ratio decreased from 0.49 to 0.45, while the mean detection probability held steady at 0.75. The SVR false alarm ratio dropping noticeably after the transition may have been expected, given the generally smaller polygons for storm-based warnings. What is remarkable is that the detection probability did not suffer at the same time. This might imply that most NWS forecasters had the skill to forecast SVR events to better than the county boundary resolution (especially for large counties) prior to the transition.

Without a doubt, there are more societal benefits given by weather radars through avenues (direct use of online data by the general public, weather forecast improvement through data assimilation, etc.) not accounted for by our models. However, these benefit models generate objective, scientifically defensible estimates based on big-data statistics; moreover, they can output gridded geospatial benefit densities that can be used for planning future radar placements.

Acknowledgments. We thank the NWS forecasters who responded to our survey about TDWR usage and also Kurt Hondl, Mike Jain, and Mark Weber for supporting this project. This paper has been approved for public release: distribution unlimited. This material is based upon work supported by the National Oceanic and Atmospheric Administration under Air Force Contract FA8702-15-D-0001. Any opinions, findings, conclusions, or recommendations expressed in this material are those of the authors and do not necessarily reflect the views of the National Oceanic and Atmospheric Administration.

REFERENCES

Andra, D. L., Jr., E. M. Quoetone, and W. F. Bunting, 2002: Warning decision making: The relative roles of conceptual models, technology, strategy, and forecaster expertise on 3 May 1999. *Wea. Forecasting*, **17**, 559–566, https://doi.org/10.1175/1520-0434(2002)017<0559:WDMTRR>2.0.CO;2.

Ashley, W. S., 2007: Spatial and temporal analysis of tornado fatalities in the United States: 1880–2005. *Wea. Forecasting*, **22**, 1214–1228, https://doi.org/10.1175/2007WAF2007004.1.

——, and A. W. Black, 2008: Fatalities associated with nonconvective high-wind events in the United States. *J. Appl. Meteor. Climatol.*, **47**, 717–725, https://doi.org/10.1175/2007JAMC1689.1.

Black, A. W., and W. S. Ashley, 2010: Nontornadic convective wind fatalities in the United States. *Nat. Hazards*, **54**, 355–366, https://doi.org/10.1007/s11069-009-9472-2.

——, and ——, 2011: The relationship between tornadic and nontornadic convective wind fatalities and warnings. *Wea. Climate Soc.*, **3**, 31–47, https://doi.org/10.1175/2010WCAS1094.1.

Brooks, H. E., and J. Correia Jr., 2018: Long-term performance metrics for National Weather Service tornado warnings. *Wea. Forecasting*, **33**, 1501–1511, https://doi.org/10.1175/WAF-D-18-0120.1.

Burgess, D. W., and L. R. Lemon, 1990: Severe thunderstorm detection by radar. *Radar in Meteorology*, D. Atlas, Ed., Amer. Meteor. Soc., 619–647.

Cho, J. Y. N., 2015: Revised Multifunction Phased Array Radar (MPAR) network siting analysis. MIT Lincoln Laboratory

Brought to you by NOAA Central Library | Unauthenticated | Downloaded 01/16/24 09:13 PM UTC

Project Rep. ATC-425, 84 pp., https://www.ll.mit.edu/sites/default/files/publication/doc/2018-05/Cho_2015_ATC-425.pdf.

——, and M. E. Weber, 2010: Terminal Doppler weather radar enhancements. *2010 IEEE Radar Conf.*, Washington, DC, IEEE, 1245–1249, https://doi.org/10.1109/RADAR.2010.5494427.

——, and J. M. Kurdzo, 2019a: Monetized weather radar network benefits for tornado cost reduction. MIT Lincoln Laboratory Project Rep. NOAA-35, 88 pp., https://www.ll.mit.edu/sites/default/files/publication/doc/monetized-weather-radar-network-benefits-cho-noaa-35.pdf.

——, and ——, 2019b: Weather radar network benefit model for tornadoes. *J. Appl. Meteor. Climatol.*, **58**, 971–987, https://doi.org/10.1175/JAMC-D-18-0205.1.

——, and ——, 2020: Weather radar network benefit model for flash flood casualty reduction. *J. Appl. Meteor. Climatol.*, **59**, 589–604, https://doi.org/10.1175/JAMC-D-19-0176.1.

Chrisman, J. N., 2013: Dynamic scanning. *NEXRAD Now*, No. 22, NOAA/NWS/Radar Operations Center, Norman, OK, 1–3, https://www.roc.noaa.gov/WSR88D/PublicDocs/NNOW/NNow22c.pdf.

——, 2014: The continuing evolution of dynamic scanning. *NEXRAD Now*, No. 23, NOAA/NWS/Radar Operations Center, Norman, OK, 8–13, http://www.roc.noaa.gov/WSR88D/PublicDocs/NNOW/NNow23a.pdf.

——, 2016: Mid-volume RESCAN of low-level elevations (MRLE): A new approach to enhance sampling of quasi-linear convective systems (QLCSs). NOAA/NWS/Radar Operations Center New Radar Technologies Doc., 21 pp., https://www.roc.noaa.gov/WSR88D/PublicDocs/NewTechnology/DQ_QLCS_MRLE_June_2016.pdf.

CIESIN, 2017: Gridded Population of the World, ver. 4 (GPWv4): Population density, rev. 10. NASA Socioeconomic Data and Applications Center, Center for International Earth Science Information Network, Columbia University, accessed 20 September 2017, https://doi.org/10.7927/H4DZ068D.

Crum, T. D., and R. L. Alberty, 1993: The WSR-88D and the WSR-88D Operational Support Facility. *Bull. Amer. Meteor. Soc.*, **74**, 1669–1688, https://doi.org/10.1175/1520-0477(1993)074<1669:TWATWO>2.0.CO;2.

DeKay, M. L., and D. H. McClelland, 1993: Predicting loss of life in cases of dam failure and flash flood. *Risk Anal.*, **13**, 193–205, https://doi.org/10.1111/j.1539-6924.1993.tb01069.x.

Doswell, C. A., III, H. E. Brooks, and M. P. Kay, 2005: Climatological estimates of daily local nontornadic severe thunderstorm probability for the United States. *Wea. Forecasting*, **20**, 577–595, https://doi.org/10.1175/WAF866.1.

DOT, 2016: Guidance on treatment of the economic value of a statistical life (VSL) in U.S. Department of Transportation Analyses—2016 adjustment. U.S. Department of Transportation Memorandum to Secretarial Officers and Modal 71 Administrators, 13 pp., https://cms.dot.gov/sites/dot.gov/files/docs/2016%20Revised%20Value%20of%20a%20Statistical%20Life%20Guidance.pdf.

FEMA, 2009: FEMA benefit-cost analysis reengineering (BCAR), version 4.5. Department of Homeland Security Doc., 75 pp., https://www.fema.gov/media-library-data/20130726-1738-25045-0690/tornadomethodology.pdf.

Fultz, A. J., and W. S. Ashley, 2016: Fatal weather-related general aviation accidents in the United States. *Phys. Geogr.*, **37**, 291–312, https://doi.org/10.1080/02723646.2016.1211854.

Goldman, A., B. Eggen, B. Golding, and V. Murray, 2014: The health impacts of windstorms: A systematic literature review. *Public Health*, **128**, 3–28, https://doi.org/10.1016/j.puhe.2013.09.022.

Hallowell, R. G., and J. Y. N. Cho, 2010: Wind-shear system cost-benefit analysis. *Linc. Lab. J.*, **18**, 47–68.

Harrison, D. R., and C. D. Karstens, 2017: A climatology of operational storm-based warnings: A geospatial analysis. *Wea. Forecasting*, **32**, 47–60, https://doi.org/10.1175/WAF-D-15-0146.1.

Heinselman, P. L., and S. M. Torres, 2011: High-temporal-resolution capabilities of the National Weather Radar Testbed Phased-Array Radar. *J. Appl. Meteor. Climatol.*, **50**, 579–593, https://doi.org/10.1175/2010JAMC2588.1.

——, D. L. Priegnitz, K. L. Manross, T. M. Smith, and R. W. Adams, 2008: Rapid sampling of severe storms by the National Weather Radar Testbed Phased Array Radar. *Wea. Forecasting*, **23**, 808–824, https://doi.org/10.1175/2008WAF2007071.1.

Hondl, K., and M. Weber, 2019: NOAA's meteorological phased array radar research program. *2019 IEEE Int. Symp. on Phased Array System and Technology (PAST)*, Waltham, MA, IEEE, 1–6, https://doi.org/10.1109/PAST43306.2019.9020994.

Istok, M. J., A. Cheek, A. D. Stern, R. E. Saffle, B. R. Klein, N. Shen, and W. M. Blanchard, 2009a: Leveraging multiple FAA radars for NWS operations. *25th Int. Conf. on Interactive Information and Processing Systems for Meteorology, Oceanography, and Hydrology*, Phoenix, AZ, Amer. Meteor. Soc., 10B.2, https://ams.confex.com/ams/pdfpapers/145466.pdf.

——, and Coauthors, 2009b: WSR-88D dual polarization initial operational capabilities. *25th Int. Conf. on Interactive Information and Processing Systems (IIPS) for Meteorology, Oceanography, and Hydrology*, Phoenix, AZ, Amer. Meteor. Soc., 15.5, https://ams.confex.com/ams/pdfpapers/148927.pdf.

Kelly, D. L., J. T. Schaefer, and C. A. Doswell III, 1985: Climatology of nontornadic severe thunderstorm events in the United States. *Mon. Wea. Rev.*, **113**, 1997–2014, https://doi.org/10.1175/1520-0493(1985)113<1997:CONSTE>2.0.CO;2.

Kurdzo, J. M., and J. Y. N. Cho, 2020: National Weather Service TDWR surveys for tornado and severe thunderstorm warning guidance. MIT Lincoln Laboratory Project Memo. 43PM-Wx-0191, 17 pp.

——, and Coauthors, 2017: Observations of severe local storms and tornadoes with the atmospheric imaging radar. *Bull. Amer. Meteor. Soc.*, **98**, 915–935, https://doi.org/10.1175/BAMS-D-15-00266.1.

Kuster, C. M., J. C. Snyder, T. J. Schuur, T. T. Lindley, P. L. Heinselman, J. C. Furtado, J. W. Brogden, and R. Toomey, 2019: Rapid-update radar observations of Z_{DR} column depth and its use in the warning decision process. *Wea. Forecasting*, **34**, 1173–1188, https://doi.org/10.1175/WAF-D-19-0024.1.

LeClerc, J., and S. Joslyn, 2015: The cry wolf effect and weather-related decision making. *Risk Anal.*, **35**, 385–395, https://doi.org/10.1111/risa.12336.

Lemon, L. R., R. J. Donaldson Jr., D. W. Burgess, and R. A. Brown, 1977: Doppler radar application to severe thunderstorm study and potential real-time warning. *Bull. Amer. Meteor. Soc.*, **58**, 1187–1193, https://doi.org/10.1175/1520-0477(1977)058<1187:DRATST>2.0.CO;2.

NWS, 2009: Verification procedures. National Weather Service Operations and Services Doc. NWSI 10-1610, 83 pp., http://www.nws.noaa.gov/directives/010/archive/pd01016001d.pdf.

Pifer, B., and H. M. Mogil, 1978: NWS hazardous weather terminology. *Bull. Amer. Meteor. Soc.*, **59**, 1583–1588, https://doi.org/10.1175/1520-0477(1978)059<1583:NHWT>2.0.CO;2.

Polger, P. D., B. S. Goldsmith, R. C. Przywarty, and J. S. Bocchieri, 1994: National Weather Service warning performance based on the WSR-88D. *Bull. Amer. Meteor. Soc.*, **75**, 203–214, https://doi.org/10.1175/1520-0477(1994)075<0203:NWSWPB>2.0.CO;2.

Brought to you by NOAA Central Library | Unauthenticated | Downloaded 01/16/24 09:13 PM UTC

Press, W. H., S. A. Teukolsky, W. T. Vetterling, and B. P. Flannery, 1992: *Numerical Recipes in C: The Art of Scientific Computing*.2nd ed. Cambridge University Press,994 pp.

Roberts, R. D., and J. W. Wilson, 1989: A proposed microburst nowcasting procedure using single-Doppler radar. *J. Appl. Meteor.*, **28**, 285–303, https://doi.org/10.1175/1520-0450(1989)028<0285:APMNPU>2.0.CO;2.

Saunders, M. E., K. D. Ash, and J. M. Collins, 2018: Usefulness of the United States National Weather Service radar display as rated by website users. *Wea. Climate Soc.*, **10**, 673–691, https://doi.org/10.1175/WCAS-D-17-0108.1.

Schmidlin, T. W., 2009: Human fatalities from wind-related tree failures in the United States, 1995–2007. *Nat. Hazards*, **50**, 13–25, https://doi.org/10.1007/s11069-008-9314-7.

Schuur, T. J., A. V. Ryzhkov, P. L. Heinselman, D. W. Burgess, and K. A. Scharfenberg, 2004: The joint polarization experiment—A summary of dual-polarization WSR-88D radar data collection and analysis. *20th Int. Conf. on Interactive Information and Processing Systems (IIPS) for Meteorology, Oceanography, and Hydrology*, Seattle, WA, Amer. Meteor. Soc., 12.1, https://ams.confex.com/ams/pdfpapers/70797.pdf.

Simmons, K. M., and D. Sutter, 2008: Tornado warnings, lead times, and tornado casualties: An empirical investigation. *Wea. Forecasting*, **23**, 246–258, https://doi.org/10.1175/2007WAF2006027.1.

——, and ——, 2011: *Economic and Societal Impact of Tornadoes*. Amer. Meteor. Soc., 282 pp.

Smith, S. B., 2011: The impact of NWS Weather Forecast Office culture on tornado warning performance. *NOAA Office of Science and Technology Seminar*, Silver Spring, MD, NWS Meteorological Development Laboratory, https://www.nws.noaa.gov/mdl/seminar/Presentations/November_30_2011.pdf.

Stensrud, D. J., and Coauthors, 2009: Convective-scale warn-on-forecast system: A vision for 2020. *Bull. Amer. Meteor. Soc.*, **90**, 1487–1500, https://doi.org/10.1175/2009BAMS2795.1.

Trapp, R. J., D. M. Wheatley, N. T. Atkins, R. W. Przybylinski, and R. Wolf, 2006: Buyer beware: Some words of caution on the use of severe wind reports in postevent assessment and research. *Wea. Forecasting*, **21**, 408–415, https://doi.org/10.1175/WAF925.1.

Weber, M. E., J. Y. N. Cho, J. S. Herd, J. M. Flavin, W. E. Benner, and G. S. Torok, 2007: The next-generation multimission U.S. surveillance radar network. *Bull. Amer. Meteor. Soc.*, **88**, 1739–1752, https://doi.org/10.1175/BAMS-88-11-1739.

——, ——, and H. G. Thomas, 2017: Command and control for multifunction phased array radar. *IEEE Trans. Geosci. Remote Sens.*, **55**, 5899–5912, https://doi.org/10.1109/TGRS.2017.2716935.

Wilson, K. A., P. L. Heinselman, C. M. Custer, D. M. Kingfield, and Z. Kang, 2017: Forecaster performance and workload: Does radar update time matter? *Wea. Forecasting*, **32**, 253–274, https://doi.org/10.1175/WAF-D-16-0157.1.

Witt, A., M. D. Eilts, G. J. Stumpf, E. D. Mitchell, J. T. Johnson, and K. W. Thomas, 1998: Evaluating the performance of WSR-88D severe storm detection algorithms. *Wea. Forecasting*, **13**, 513–518, https://doi.org/10.1175/1520-0434(1998)013<0513:ETPOWS>2.0.CO;2.

Brought to you by NOAA Central Library | Unauthenticated | Downloaded 01/16/24 09:13 PM UTC